Iraqi Journal of Computers, Communications, Control and Systems Engineering

Volume 26 | Issue 1 Article 7

4-4-2026

Design and Implementation of an OFOPID Controller for Iraqi Two Areas Power System Using Ant-Colony Optimization Algorithm

Mazin N. Ajaweed
University of Technology, Al-Sinaa Street, College of Artificial Intelligence Engineering,
mazin.n.ajaweed@uotechnology.edu.iq

Abbas H. Issa
University of Technology, Al-Sinaa Street, College of Artificial Intelligence Engineering,
mazinthany2004@gmail.com

Mazin T. Muhssin
Mustansiriyah University, Bab-Almadhem, Baghdad, Iraq

IJCCCE 2026;26(1):83–100

RESEARCH ARTICLE

Design and Implementation of an OFOPID Controller for Iraqi Two Areas Power System Using Ant-Colony Optimization Algorithm

Mazin N. Ajaweed [a,*], Abbas H. Issa [a], Mazin T. Muhssin [b]

[a] University of Technology, Al-Sinaa Street, College of Artificial Intelligence Engineering
[b] Mustansiriyah University, Bab-Almadhem, Baghdad, Iraq

ABSTRACT

This study introduces a multi-zone of the Iraqi system model powered by various energy sources, where decentralized controllers operate independently to manage the system's frequency. The system model comprises two zones: the first zone represents the north and central power plants of Iraq. The second zone incorporates the Euphrates and southern power plants of Iraq. The data of the system is obtained from the Iraqi Ministry of Electricity. To evaluate the system's performance, a load disturbance is applied to the system. The study examines various control methodologies, first with an Optimised Proportional-Integral-Derivative (OPID) controller as the baseline, subsequently progressing to an Optimised Fractional Order (OFOPID) controller. These controllers are utilized to maintain the frequency of each zone around 50 Hz and maintain the power of Tie-lines between the zones at schedualled values. The parameters of the controllers are refined using the Ant-Colony Optimization (ACO) Algorithm. Three case studies are conducted. In the first and second case studies, 10% of load disturbance is subjucted individually to the first and second zones, respectively. In the third case study, the 10% of load disturbance is given for both zones simultaneously. Simulation results show that improvement about 97%, 85% for settling time and peak respectively in area1 and 94%, 97% in area2 respectively in comparison with classical PID controllers and using Iraqi dataset.

Keywords: Two area, Iraqi power system, OFOPID, Ant-Colony optimization

Received 21 September 2025; revised 13 November 2025; accepted 20 November 2025.
Available online 4 April 2026

* Corresponding author.
E-mail addresses: mazin.n.ajaweed@uotechnology.edu.iq (M. N. Ajaweed), abbas.h.issa@uotechnology.edu.iq (A. H. Issa), mazinthany2004@gmail.com (M. T. Muhssin).

https://doi.org/xx.xxxxx/2617-3352.1519

Highlights

1. Iraqi two areas interconnected power system.
2. Optimized PID Controller.
3. Optimized fractional order PID Controller.
4. ACO with ten parameters.
5. Robust and Stable frequency.

1. Introduction

The main purpose of Automatic Generation Control (AGC) is to perform load frequency control (LFC), which is regarded as one of the most critical control challenges in the design and operation of any electrical power system [1, 2]. In any power system, LFC serves two key functions: maintaining system frequency and regulating power exchange with neighboring areas at predetermined values [3–6]. These objectives are achieved by monitoring the area control error (ACE), an error signal that represents the imbalance between actual load demand and generated power [7, 8]. Frequency control in power systems is generally structured into three hierarchical levels: primary, secondary, and tertiary control. The primary frequency control loop works to arrest frequency decline before under- or over-frequency protection relays are triggered [9, 10]. This is usually implemented through the governor droop characteristic, which, however, introduces steady-state errors [11].

The secondary control level referred to as LFC or AGC is tasked with regulating system frequency and has two main goals: (i) keeping the frequency within an acceptable range, and (ii) managing power flows on the main tie-lines between interconnected control areas [12-15]. The tertiary control level focuses on redispatching generation units and mobilizing reserves after significant disturbances. A power system is typically composed of interconnected control areas (CAs), each representing a coordinated group of generators. These CAs are linked together through tie-lines that enable power exchange [16, 17]. The following paraghraphs summarizes several approaches proposed by researchers for implementing AGC.

Manoj k. et al. (2020) [18] An adaptive artificial neural network (ANN) optimized proportional-integral-derivative (PID) controller is proposed for the examination of load frequency control (LFC) in a system incorporating distributed generation (DG) resources. The diverse distributed generation resources comprise wind turbine generators (WTG), battery energy storage systems (BESS), aqua electrolyzers (AE), diesel engine generators (DEG), and fuel cells (FC). Kumar et al. (2021) [19] developed an SMC-based design for regulating frequency deviations in interconnected power systems. The sliding surface parameters were tuned using Particle Swarm Optimization (PSO) and Grey Wolf Optimization (GWO) algorithms. Using GWO resulted in an 88.91% performance improvement, and the system maintained good response under random disturbances. Jalal N. et al. (2021) [20] applied an intelligent fuzzy PID controller to multi-area power systems experiencing disturbances and uncertainties. The fuzzy rule weights and membership functions were optimized using the Trip-DE algorithm. For a two-area system, the controller achieved an ITAE value of about 0.0108 and a maximum undershoot of 0.0210 Hz, delivering robust and high-performance results. Gupta N. et al. (2022) [21] optimized a PID controller using the Jaya algorithm for a two-area system incorporating gas, hydro, and thermal power sources. The method effectively enhanced the performance of slower hydro units by

increasing the contribution from gas and thermal generation. Boopathi D. et al. (2023) [22] The PID controller is suggested as a secondary controller to stabilize system performance during abrupt power system demands. The particle swarm optimization (PSO) algorithm is employed to derive optimal gain values for the suggested PID controller. Mohamed B. (2023) [23] This study utilizes chaos game optimization (CGO), a robust optimization method, to effectively build a novel cascade AFOFPID controller for four interconnected power systems (IPSs) to address load-frequency control (LFC) challenges. Wang P. et al. (2024) [24] introduced a Optimized fractional order PID (OFOPID) controller optimized using the Improved Gradient-Based Optimizer (IGBO) for a two-area system with both conventional and renewable energy sources. The controller showed excellent robustness against load variations and renewable fluctuations.

Our problem statement is to design AGC system for regulating the power output of different generating stations according to pre-determined parameters and cover the load disturbances in a particular area without takeing into account the load disturbances in the neighbuoring area. In this study, controller gains were determined using the ACO and the performance was compared against optimized fractional order OFOPID controller in a multi-area power system featuring diverse generation sources in each area. The key contributions of this work include:

1. Developing a model of the Iraqi power system a first-of-its-kind effort in AGC-related research for Iraq designed to be adaptable for future integration of renewable energy sources.
2. Utilizing authentic data obtained from the Iraqi Ministry of Electricity, in collaboration with international partners, to formulate a strategic roadmap for the country's power system development.
3. This study includes generation source models with a deadband constraint to regulate governor speed. The speed governor may not respond instantly to changes in the input signal until it attains a predetermined threshold. This practical constraint has been neglected in the majority of prior power system studies.
4. This study examines nonlinear dynamics by incorporating a hysteresis pattern into the governor-turbine system model for each generation source. The designated upper and lower limits represent the maximum and minimum velocities for the operation of the control valves (gates).
5. While the conventional AGC (Automatic Generation Control) typically employs a PI controller, this study explores, for the first time in the context of the Iraqi power system, the application of a fractional-order PID controller.

The outline of paper is organized as follows. The section two includes the power system modeling for first and second areas then section three contains design OPID, OFOPID controllers. Section four simulation and results then finally section five conclusion and future work.

2. Iraqi power system model

The Iraqi power system is confronted with significant challenges, especially in the generation and transmission sectors, driven by the continuous growth in load demand and the limited number of power plants. This situation highlights the need for greater focus and research in the field. In this study, attention is directed toward the Automatic Generation

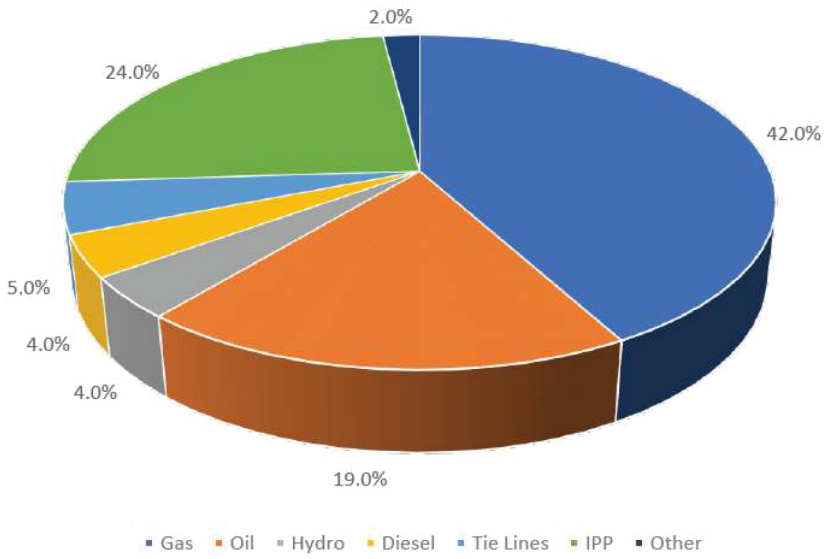

Fig. 1. Iraqi generation plants [25].

Control (AGC) sector to ensure stable frequency regulation in the face of load variations. The Iraqi grid depends mainly on four types of power plants: gas, diesel, thermal, and hydro. Geographically, the system is divided into four regions north, center, euphrates, and south. For the purposes of this work, these have been consolidated into two main regions: Region One, comprising the northern and central plants, and Region Two, covering the Euphrates and southern plants. Each plant operates within a limited generation capacity and is affected by factors such as extreme temperatures, climatic conditions, and sudden load changes, all of which can disrupt generation frequency. This makes implementing load frequency control essential for maintaining system stability. Fig. 1 illustrates the share of generation for each plant type based on data from the official report of the Iraqi Ministry of Electricity [25].

2.1. Mathematical model of area one

Hydro, thermal, gas, and diesel generation sources are included, and the state-space model for the first region is expressed as follows:

$$\dot{x} = A_1 x + B_1 u_1 - d_1 \tag{1}$$

Where:
x = the vector states of the system (1×11)
u_1 = the control signal vector (1×11)
d_1 = the disturbance vectors (11×1)
A_1 = the system input states (11×11)
B_1 = The input vector states (11×1)

The overall all state space system is given in Eq. (2).

Where:

$$\begin{bmatrix}\dot{x}_1\\ \dot{x}_2\\ \dot{x}_3\\ \dot{x}_4\\ \dot{x}_5\\ \dot{x}_6\\ \dot{x}_7\\ \dot{x}_8\\ \dot{x}_9\\ \dot{x}_{10}\\ \dot{x}_{11}\end{bmatrix} = \begin{bmatrix} \frac{-1}{8.5} & \frac{-1}{8.5} & \frac{1}{8.5} & \left(-2+\frac{2*5}{38}\right)\left(\frac{1}{8.5}\right) & \frac{-2*5*1}{38*8.5} & \frac{1}{8.5} & 0 & \frac{1}{8.5} & 0 & \frac{1}{8.5} & 0\\ 0.2 & 0 & 0 & 0 & 0 & 0 & 0 & 0 & 0 & 0 & 0\\ 0 & 0 & \frac{-2}{1} & \left(\frac{-5}{38}+1\right)*\frac{2}{1} & \frac{2*5}{38*1} & 0 & 0 & 0 & 0 & 0 & 0\\ 0 & 0 & 0 & \frac{-1}{38} & \frac{1}{38} & 0 & 0 & 0 & 0 & 0 & 0\\ \frac{-1}{0.05*0.2} & 0 & 0 & 0 & \frac{-1}{0.2} & 0 & 0 & 0 & 0 & 0 & 0\\ 0 & 0 & 0 & 0 & 0 & \frac{-1}{0.3} & \frac{1}{0.3} & 0 & 0 & 0 & 0\\ \frac{-1}{0.05*0.08} & 0 & 0 & 0 & 0 & 0 & \frac{-1}{0.08} & 0 & 0 & 0 & 0\\ 0 & 0 & 0 & 0 & 0 & 0 & 0 & \frac{-1}{0.3} & \frac{1}{0.3} & 0 & 0\\ \frac{-1}{0.05*0.2} & 0 & 0 & 0 & 0 & 0 & 0 & 0 & \frac{-1}{0.2} & 0 & 0\\ 0 & 0 & 0 & 0 & 0 & 0 & 0 & 0 & 0 & \frac{-1}{0.2} & \frac{1}{0.2}\\ \frac{-1}{0.05*0.05} & 0 & 0 & 0 & 0 & 0 & 0 & 0 & 0 & 0 & \frac{-1}{0.05}\end{bmatrix} x$$

$$+ \begin{bmatrix}0\\0\\0\\0\\\frac{1}{0.2}\\0\\\frac{1}{0.08}\\0\\\frac{1}{0.2}\\0\\\frac{1}{0.05}\end{bmatrix} u1 - \begin{bmatrix}\frac{1}{8.5}\\0\\0\\0\\0\\0\\0\\0\\0\\0\\0\end{bmatrix} d_1 \tag{2}$$

$T_r, T_2, T_1, T_w, T_{th1}, T_{th2}, T_{gas1}, T_{gas2}, T_{d1}, T_{d2}$ are the governor-turbine time constants in seconds.

R = governor droop gain
K_p = power system gain
T_p = power system time constant in seconds

2.2. Mathematical model of area two

The second region corresponds to Iraq's southern and Euphrates areas, comprising thermal, gas, and diesel power plants, but lacking a hydropower facility unlike the first region. The variation of frequency in this region is denoted by Δf_2, and the governor droop settings as well as the time constants for the gas, diesel, and thermal units are the same as those applied in the first region. The state-space model for the second region is given in Eqs. (3) and (4).

$$\dot{x} = A_2 x + B_2 u_2 - d_2 \tag{3}$$

Where:
x = the vector states of the system (1×8)

u_2 = the control signal vector (1×8)

$$\begin{bmatrix}\dot{x}_1\\ \dot{x}_2\\ \dot{x}_3\\ \dot{x}_4\\ \dot{x}_5\\ \dot{x}_6\\ \dot{x}_7\\ \dot{x}_8\\ \dot{x}_9\\ \dot{x}_{10}\\ \dot{x}_{11}\end{bmatrix} = \begin{bmatrix} \frac{-1}{8.5} & \frac{-1}{8.5} & \frac{1}{8.5} & \left(-2+\frac{2*5}{38}\right)\left(\frac{1}{8.5}\right) & \frac{-2*5*1}{38*8.5} & \frac{1}{8.5} & 0 & \frac{1}{8.5} & 0 & \frac{1}{8.5} & 0\\ 0.2 & 0 & 0 & 0 & 0 & 0 & 0 & 0 & 0 & 0 & 0\\ 0 & 0 & \frac{-2}{1} & \left(\frac{-5}{38}+1\right)*\frac{2}{1} & \frac{2*5}{38*1} & 0 & 0 & 0 & 0 & 0 & 0\\ 0 & 0 & 0 & \frac{-1}{38} & \frac{1}{38} & 0 & 0 & 0 & 0 & 0 & 0\\ \frac{-1}{0.05*0.2} & 0 & 0 & 0 & \frac{-1}{0.2} & 0 & 0 & 0 & 0 & 0 & 0\\ 0 & 0 & 0 & 0 & 0 & \frac{-1}{0.3} & \frac{1}{0.3} & 0 & 0 & 0 & 0\\ \frac{-1}{0.05*0.08} & 0 & 0 & 0 & 0 & 0 & \frac{-1}{0.08} & 0 & 0 & 0 & 0\\ 0 & 0 & 0 & 0 & 0 & 0 & 0 & \frac{-1}{0.3} & \frac{1}{0.3} & 0 & 0\\ \frac{-1}{0.05*0.2} & 0 & 0 & 0 & 0 & 0 & 0 & 0 & \frac{-1}{0.2} & 0 & 0\\ 0 & 0 & 0 & 0 & 0 & 0 & 0 & 0 & 0 & \frac{-1}{0.2} & \frac{1}{0.2}\\ \frac{-1}{0.05*0.05} & 0 & 0 & 0 & 0 & 0 & 0 & 0 & 0 & 0 & \frac{-1}{0.05}\end{bmatrix} x$$

$$+\begin{bmatrix}0\\0\\0\\0\\\frac{1}{0.2}\\0\\\frac{1}{0.08}\\0\\\frac{1}{0.2}\\0\\\frac{1}{0.05}\end{bmatrix} u1 - \begin{bmatrix}\frac{1}{8.5}\\0\\0\\0\\0\\0\\0\\0\\0\\0\\0\end{bmatrix} d_1$$

d_2 = the disturbance vectors (8×1)
A_2 = the system input states (8×8)
B_2 = The input vector states (8×1)
The overall all state space system can be summarized as follow in Eq. (4).

$$\begin{bmatrix}\dot{x}_{12}\\ \dot{x}_{13}\\ \dot{x}_{14}\\ \dot{x}_{15}\\ \dot{x}_{16}\\ \dot{x}_{17}\\ \dot{x}_{18}\\ \dot{x}_{19}\end{bmatrix} = \begin{bmatrix} \frac{-1}{7.83} & \frac{-1}{7.83} & \frac{1}{7.83} & 0 & \frac{1}{7.83} & 0 & \frac{1}{7.83} & 0\\ 0.2 & 0 & 0 & 0 & 0 & 0 & 0 & 0\\ 0 & 0 & \frac{-1}{0.3} & \frac{1}{0.3} & 0 & 0 & 0 & 0\\ \frac{-1}{0.05*0.08} & 0 & 0 & \frac{-1}{0.08} & 0 & 0 & 0 & 0\\ 0 & 0 & 0 & 0 & \frac{-1}{0.3} & \frac{1}{0.3} & 0 & 0\\ \frac{-1}{0.05*0.2} & 0 & 0 & 0 & 0 & \frac{-1}{0.2} & 0 & 0\\ 0 & 0 & 0 & 0 & 0 & 0 & \frac{-1}{0.2} & \frac{1}{0.2}\\ \frac{-1}{0.05*0.05} & 0 & 0 & 0 & 0 & 0 & 0 & \frac{-1}{0.05}\end{bmatrix} x + \begin{bmatrix}0\\0\\0\\\frac{1}{0.08}\\0\\\frac{1}{0.2}\\0\\\frac{1}{0.05}\end{bmatrix} u2 - [0]\ d_2 \quad (4)$$

Where:
$T_{th1},\ T_{th2},\ T_{gas1},\ T_{gas2},\ T_{d1},\ T_{d2}$ = governor-turbine time constants in seconds.
R = governor droop gain
K_p = power system gain
T_p = power system time constant in seconds

$$H_{eq} = \sum_{i}^{N} H_i.\ \frac{S_i}{S_{zone}} \quad (5)$$

$$B = \frac{1}{R} + D \quad (6)$$

2.3. The overall mathematical model

Following the explanation of the mathematical model for each region, the parameters including frequency bias coefficient (B), Tie-line power coefficient (Kij), damping coefficient (D), and inertia (H) can now be substituted as listed in Table 1. These values are derived from the specifications of the Iraqi power system. The inertia (H) and bias coefficient (B) for each region were calculated using Eqs. (5) and (6) [26]:

Table 1. Generators and system model parameters [13].

Membrane	Area 1	Area 2	Tie-Line
T_r	-	5s	-
T_1	-	0.2s	-
T_2	-	38s	-
T_w	-	1s	-
T_{gas1}	0.3s	0.3s	-
T_{gas2}	0.2s	0.2s	-
T_{d1}	0.2s	0.2s	-
T_{d2}	0.05s	0.05s	-
T_{th1}	0.3s	-	-
T_{th2}	0.08s	-	-
R	0.05 Hz/Mw	0.05 Hz/Mw	-
D	1 Hz	1 Hz	-
H_{eq}	8.5 (s pu)	7.8394 (s pu)	-
B	21 Mw/Hz	21 Mw/Hz	-
K_{12}&K_{21}	-	-	0.2 Mw/Hz

Here, H_i denotes the equivalent inertia constant for each generating station based on its fuel type, S_i is the rated capacity of each generating station, S_{zone} represents the total rated capacity of the respective zone, and N is the total number of generating stations. The parameter (B) refers to the frequency bias constant, which is assigned a value of 21 in accordance with Eq. (6) above. Fig. 2 illustrate the simplified interconnected Iraqi power system model for the first and second zones, respectively, after incorporating the inertia values (H_i) and the bias coefficient (B). For analyzing frequency response and conducting simulations, the system's nonlinear dynamics can be modeled by adding saturation characteristics and dead-band limits to the. governor–turbine model, as depicted in Fig. 2. The specified upper and lower limits correspond to the maximum and minimum speeds for opening and closing the control valves.

3. Controller design

Fractional calculus has been explored for over three centuries because of its extensive applications across scientific and engineering disciplines. It is based on the concept of integrals and derivatives of non-integer (positive real) orders [27–29].

3.1. Grunwald-Letnikov definition

The Grunwald–Letnikov definition given below is useful in fractional differential equations for obtaining effective numerical solutions [27–29]:

$$aD_t^{\alpha} = \lim_{h \to 0} \frac{1}{h^{\alpha}} \sum_{r=0}^{\left[\frac{t-a}{h}\right]} -1^r \binom{n}{r} f\left(t - rh\right) \tag{7}$$

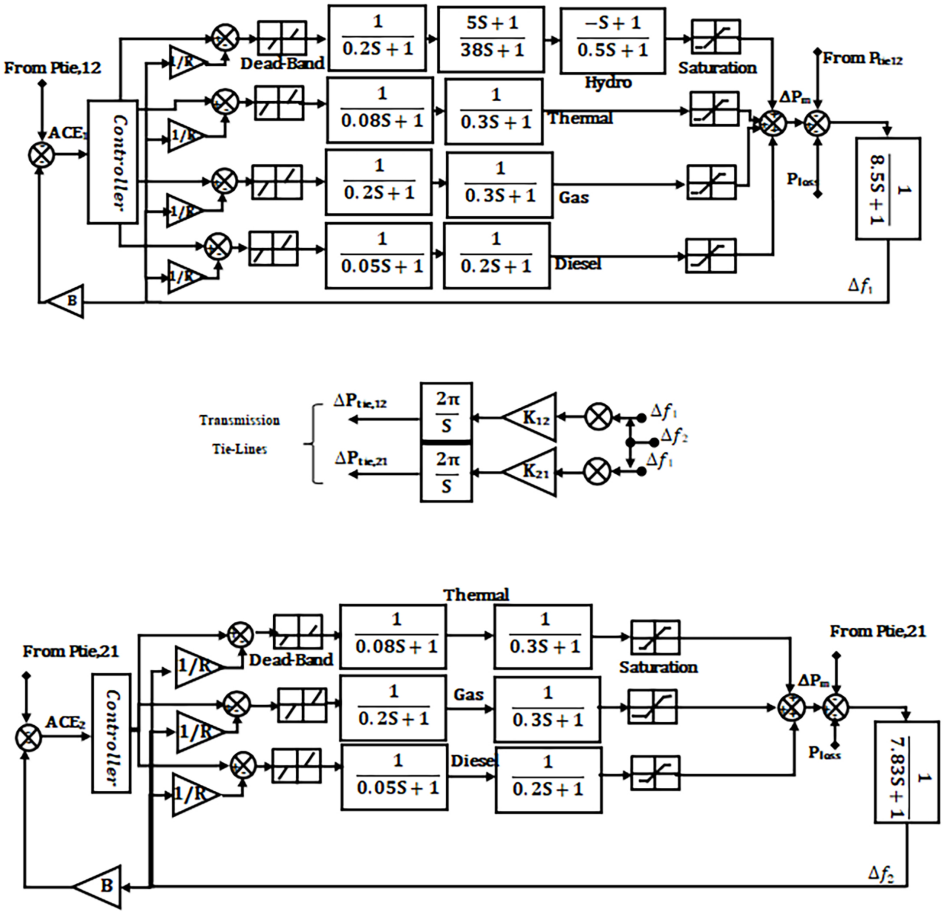

Fig. 2. Simplified interconnected iraqi power system model.

Where, n is an integer, a and t are the operator limits, $[\frac{t-a}{h}]$ represents the integer component and α is subjected to n-1 < α < n, r and n is the binomial coefficient expressed as:

$$\binom{n}{r} = \frac{\Gamma(n+1)}{\Gamma(r+1).\Gamma(n-r+1)} \tag{8}$$

The Gamma Equation function above is expressed as follow:

$$\Gamma(x) = \int_0^{\infty} t^{x-1}.e^{-t}dt,\ R(z) > 0 \tag{9}$$

3.2. Riemann-Liouville definition

The Riemann–Liouville definition applies fractional operators for solving differential equations and integrating arbitrary numbers It is expressed as follows [27–29]:

$$aD_t^{\alpha} = D^n.J^{n-a}.f(t) = \frac{1}{\Gamma(n-\alpha)}.\left(\frac{d}{dt}\right)^n.\int_a^t \frac{f(\tau)}{(t-\tau)^{\alpha-n+1}}.d\tau \tag{10}$$

where, n is an integer, α is a real number subjected to $n-1 < \alpha < n$, J is the integral operator and t, a are the limits of integration.

3.3. Optimized fractional order PID controller (OFOPID)

Proportional-Integral-Derivative (PID) control is one of the most widely used forms of control in the industry but has limitations under parameter variations and uncertainties. Optimized Fractional-order PID (OFOPID) control, initially introduced by Podlubny, provides enhanced flexibility in tuning gain and phase characteristics and demonstrates improved robustness against gain variations. This controller is typically expressed in the form PI^{α} D^{β} controller. The standard mathematical expression for the OFOPID controller is given as follows [27–29]:

$$C(s) = K_p + k_i s^{-\alpha} + k_d s^{\beta} \tag{11}$$

Where (α) and (β) denote the fractional orders of integration and differentiation respectively, their values typically range between 0 and 1. When both $\alpha = 1$ and $\beta = 1$, the controller reduces to the classical PID form. If α is set to 0, the controller becomes a fractional PD controller, and when $\alpha = 0$ and $\beta = 1$, it simplifies further to the conventional integer-order PD controller. On the other hand, setting $\beta = 0$ results in a fractional PI controller, and with $\beta = 0$ and $\alpha = 1$, it becomes the standard PI controller. Accordingly, traditional PI, PD, and PID controllers can be viewed as particular instances of the more general fractional-order controllers. While fractional PI and PD controllers allow for tuning based on three design specifications, the optimized fractional-order PID (OFOPID) controller introduces two extra tuning parameters α and β in addition to the conventional gains (k_p, k_i, k_d). This provides the OFOPID with the ability to meet five tuning requirements which could significantly enhance the control flexibility. The block diagram of OFOPID shown below in Fig. 3.

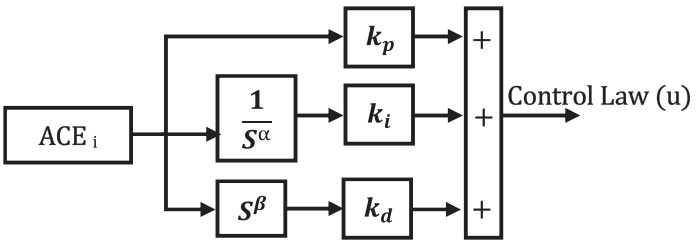

Fig. 3. Block diagram of OFOPID controller.

4. Ant-Colony optimization (ACO) algorithm

Metaheuristic optimization methods offer efficient and cost-effective means for adjusting fractional controllers. These techniques rely on an objective function to asses solution performance and determine the optimal parameter values [30]. In this research the optimization algorithm is used Ant Colony Optimization technique (ACO) to tune the three parameters of classical OPID and five parameters of fractional OFOPID controller to improve the response of the system. The cost function depicated in Eq. (12) below is chosen to minimize the Area Control Error (ACE) Eqs. (13) and (14) for each area to be zero error by the integration of the summation of the square area control error for both

area one (ACE_1) and area two (ACE_2) multiplied by the time (t).

$$Cost\ value = \int_0^{\infty} (t.ACE_1{}^2 dt + t.ACE_2{}^2 dt) \tag{12}$$

In this algorithm, the groups of ants are randomly searching for their target in the space of the problem. In single zone, the tuning of the controller is only required to regulate the grid frequency. For an interconnected system, however, the tuning of the controller is required to achieve multiple objectives, i.c, regulate the zonal frequency and coordinate the net exchanged across the tie-lines. To achieve these objectives, a composite performance metric called the Area Control Error (ACE) is employed as the feedback variable in the control loop which combines two key components: the zonal frequency deviation (weighted by the area's frequency bias factor) and the deviation of actual tie-line flows from their schedualled values. Thus, minimizing the ACE through the cost function can achieve these two aims by reducing the ITSE value of the cost function (12) to its lowest value. The ACO steps for finding the optimal values of OPID and OFOPID parameters $k_{p(OPID)}$, $k_{i(OPID)}$, $k_{d(OPID)}$, $\alpha_{(OFOPID)}$, $\beta_{(OFOPID)}$, $k_{p(OFOPID)}$, $k_{i(OFOPID)}$, $k_{d(OFOPID)}$ are summarized as follows:

- ➢ Define the multi-area model shown in Fig. 2 and ACO parameters in Table 2.
- ➢ Establish pheromone trails on all potential solution components, often configured uniformly.
- ➢ Configure algorithm parameters (quantity of ants, pheromone decay rate, effect coefficients alfa and beta, maximum iterations).
- ➢ Each ant constructs a solution incrementally.
- ➢ At every decision juncture, ants select the subsequent alternative depending on:

Pheromone intensity (the desirability of a path in previous rounds).
Heuristic information (domain-specific knowledge, such as the inverse of distance in TSP).

- ➢ The likelihood of choosing an option is a weighted equilibrium of pheromonal and heuristic influences.
- ➢ Upon the completion of their solutions, assess them utilizing the cost function in (12).
- ➢ Monitor the optimal solution identified to date.pheromonal and heuristic elements.
- ➢ Evaporation: diminish all pheromone concentrations to prevent excessive buildup and promote exploration.
- ➢ Ants deposit pheromones on the components of the solutions they utilize, with a greater quantity of pheromone allocated to superior solutions, which is inversely related to the cost of the solution.
- ➢ Reiterate the solution construction and pheromone updating procedures for several iterations or until a termination requirement is satisfied (e.g., convergence, maximum iterations, or satisfactory solution quality).

Ant Colony Optimization (ACO) is favored for discrete, combinatorial, and graph-based optimization challenges where path construction and retention of effective solutions are significant. For continuous or high-dimensional problems, techniques such as Particle Swarm Optimization (PSO), Differential Evolution (DE), or Genetic techniques (GA) are frequently more effective. The flowchart of ACO is illustrated Fig. 4 [31].

The Area Control Error (ACE) for the two areas are:

$$For\ area\ one\ ACE1\ (t) = \left(2.\pi.K_{12}.\left(\Delta f_1 - \Delta f_2\right) + B_1.\Delta f_1\right) \tag{13}$$

Table 2. ACO parameters through all cases.

Method	Value
Number of Ants	100
Alpha	0.8
Beta	0.2
Evaporation rate	0.7
Initial pheromone	0.01
Max Iterations	100
Stopping critera	Summation of areas control error

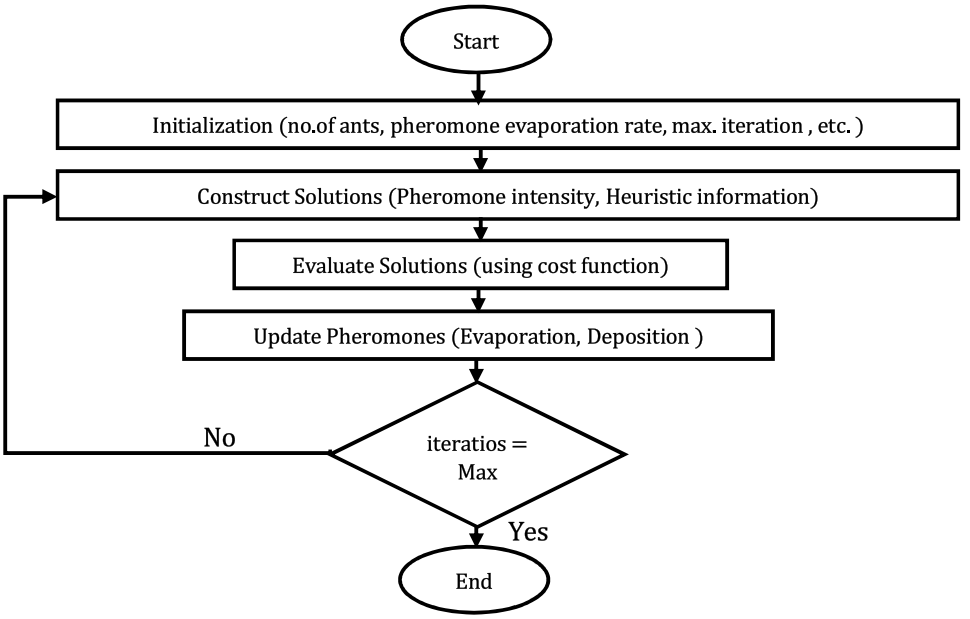

Fig. 4. ACO flowchart.

$$For\ area\ two\ ACE2\,(t) = -\left(2.\pi.K_{21}.\left(\Delta f_1 - \Delta f_2\right) + B_2.\Delta f_2\right) \tag{14}$$

The coefficient K_{12} denotes the synchronizing power factor between the two areas, while the expression $2\pi.K_{12}.(\Delta f_1 - \Delta f_2)$ & $-2\pi.K_{21}.(\Delta f_1 - \Delta f_2)$ represents the deviation of actual tie-line power exchange from the scheduled value with the neighboring area. The terms $B_1\Delta f_1$ and $B_2\Delta f_2$ correspond to the frequency bias contributions of areas one and two, respectively.

5. Simulation results and discussion

In this section, two-area interconnected power system is considered for the simulation. The response obtained with the proposed method is compared with the recently reported methods in the literature. The performance has been evaluated in terms of peak value, settling time, overshoot values. All simulations were performed through MATLAB simulimnk 2019.

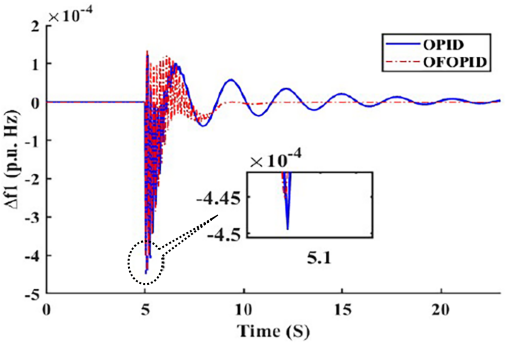

Fig. 5. Frequency deviation in area 1 for case 1.

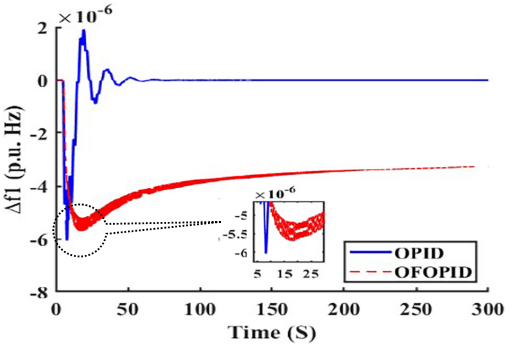

Fig. 6. Frequency deviation in area 2 for case 1.

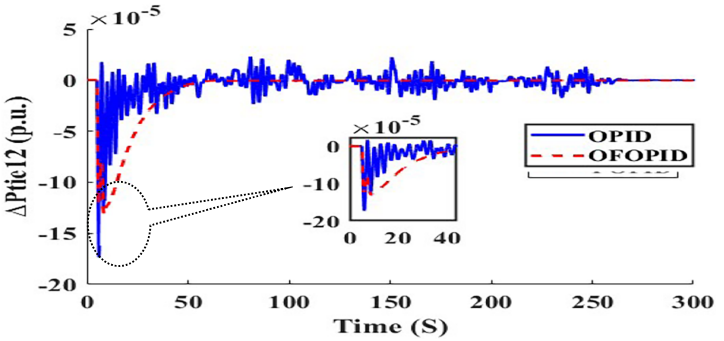

Fig. 7. Tie-line interconnection power exchange for case 1.

5.1. Case study 1

In case study 1, a sudden load disturbance of 0.1 p.u. was applied to area 1 at time t = 5 seconds to asses the performance of the proposed approach through simulation in a two-areas power system. Figs. 5 to 7 illustrate the resulting frequency deviations in areas 1 and 2, along with the power flow across the tie-line connecting the two zones under this scenario. The system's response was compared to that of a traditional OPID controller tuned using the Ant Colony Optimization (ACO) technique as in Table 3. Despite the load disturbance in case study 1 limited to area 1, the frequency responses of both area 1 and area 2 are displayed to demonstrate the inter-area coupling effect. The tie-line power exchange across the regions results in disturbances in area 1 effecting the frequency of area 2. Thus the frequency regulation of area 1 and area 2 illustrates the suggested controller's ability to sustain the specified frequency stability throughout the interconnected system.

Fig. 7 depicts the transient fluctuation of the tie-line power exchange between area 1 and area 2 subsequent to a load disturbance in area 1. The initial negative deviation indicates an abrupt power shortfall in area 1, resulting in power transfer from area 2 via the tie-line. The oscillatory transient represents the inter-area coupling and the control system's effort to restore frequency and power equilibrium between the two areas. The fast attenuation and smooth convergence to zero indicate that the suggested controller successfully mitigates inter-area oscillations and guarantees coordinated stability of the interconnected system.

Table 3. Comparsion analysis for case study 1.

Method	Peak Value	Settling time (s)	Rising Time t_r (s)	Area
OPID	-4.495×10^{-4} p.u. Hz	18.1589	3.8498×10^{-6}	1
OFOPID	-4.45×10^{-4} p.u. Hz	8.8069	2.1277×10^{-5}	1
OPID	-7.897×10^{-6} p.u. Hz	399.9967	0.0190	2
OFOPID	-6.9×10^{-6} p.u. Hz	218.9365	0.0649	2
$\Delta P_{Tie\text{-}12OPID}$	-0.0007×10^{-5} p.u.	319.4177	0.006	–
$\Delta P_{Tie\text{-}12OFOPID}$	-0.0001×10^{-5} p.u.	54.6195	0.004	–

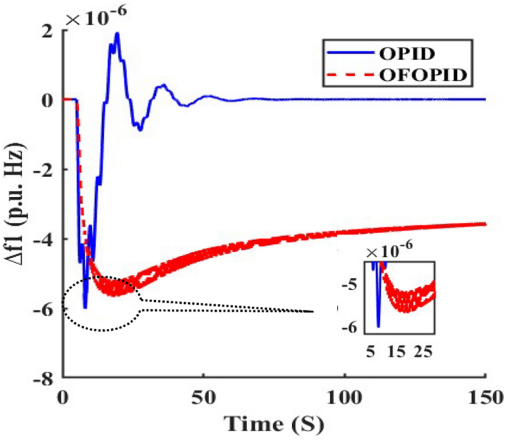

Fig. 8. Frequency regulation in area 1 for case 2.

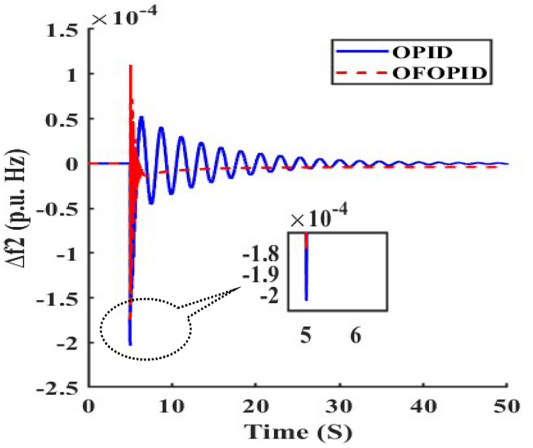

Fig. 9. Frequency regulation in area 2 for case 2.

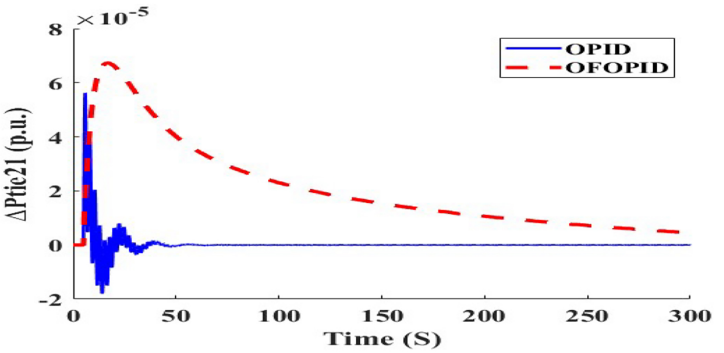

Fig. 10. Tie-line interconnection for case 2.

5.2. Case study 2

In case study 2, a sudden load disturbance of 0.1 p.u. was applied to area 2 at time t = 5 seconds to assess the performance of the proposed approach through simulation in a two-area power system. Figs. 8 to 10 illustrate the resulting frequency deviations in area 1 and 2, along with the power flow across the tie-line connecting the two zones under this scenario. The system's response was compared to that of a traditional OPID controller tuned using the Ant Colony Optimization (ACO) technique as in Table 4. The comparison demonstrated that the proposed OFOPID controller achieved a faster dynamic response and a lower peak deviation in frequency regulation.

Table 4. Comparsion analysis for case study 2.

Method	Peak Value	Settling time (s)	Rising time t_r (s)	Area
OPID	-6.01×10^{-6} p.u.Hz	45.7978	1.6638×10^{-5}	1
OFOPID	-5.678×10^{-6} p.u.Hz	375.2	1.1778	1
OPID	–0.0002 p.u.Hz	27.824	2.862×10^{-5}	2
OFOPID	–0.0001 p.u.Hz	13.19	1.8907×10^{-4}	2
$\Delta P_{Tie\text{-}21OPID}$	-1.902×10^{-5} p.u.	41.47	1.01×10^{-4}	–
$\Delta P_{Tie\text{-}21OFOPID}$	6.95×10^{-5} p.u.	305.33	0.0137	–

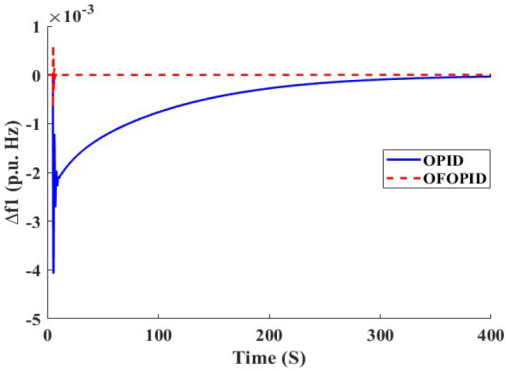

Fig. 11. Frequency regulation in area 1 for case 3.

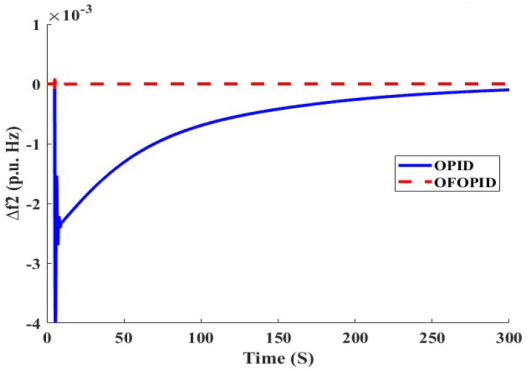

Fig. 12. Frequency regulation in area 2 for case 3.

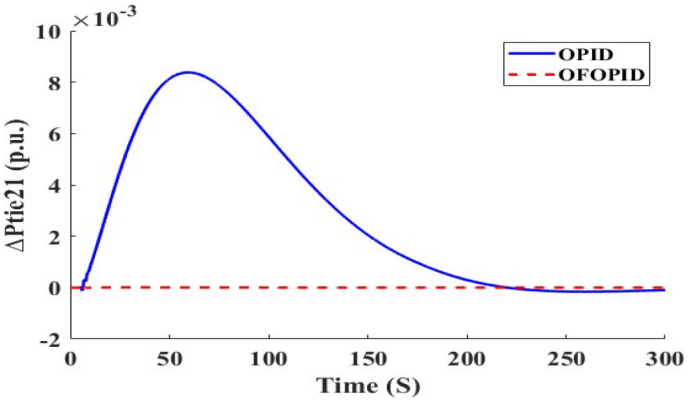

Fig. 13. Tie-line interconnection for case 3.

5.3. Case study 3

In case study 3, area 1 and area 2 undergoing 0.1 p.u. unit step load simultaneously is taken to illustrate the performance of the proposed method through simulation results. Figs. 11 to 13 show the frequency regulation in area 1, area 2, and tie-line interconnection respectively.

5.4. Case study 4

In case study 4, the controller experienced a 15% uncertainty in the power synchronisation coefficients K_{12} and K_{21} to evaluate its robustness, in addition to the previously assessed cases. Figs. 14 and 15 illustrate the controller's efficacy in sustaining the requisite

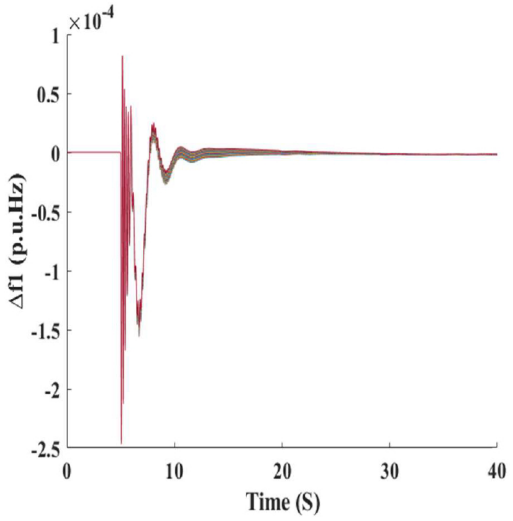

Fig. 14. Frequency regulation in area1 for case study 4 (k12 = 15% uncertainty).

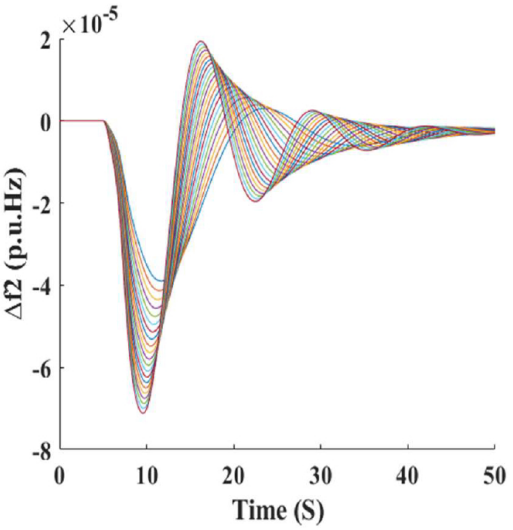

Fig. 15. Frequency regulation in area2 for case study 4 (k21 = 15% uncertainty).

system frequency, avoiding large drops, and ensuring the frequency remains within the allowed range.

6. Comparitive study with other relevant works for two areas interconnected power system

This section is carried out to provide a comprehensive comparsion of our study with literature. Table 6 is conducted to include the comared specifications.

The comparative table illustrates the (OFOPID) controller's superiority for realistic performance and robustness in managing abrupt load variations across one or several zones simultaneously. This superiority was based on two factors: first, the values obtained from the system, as indicated in Table 5, and second, the implementatin of constraints that impart nonlinear characteristics to the model and controller by incorporating dead-band and saturation limits into the generation system, which are often excluded in most research studies and consequently influence overall system performance.

Table 5. Comparsion analysis for case study 3.

Method	Peak Value	Settling time (s)	Rising Time t_r (s)	Area
OPID	–0.004 p.u. Hz	283.1	0.002	1
OFOPID	–0.0006 p.u.Hz	8.3	1.77×10^{-5}	1
OPID	–0.0039 p.u.Hz	285.7	0.002	2
OFOPID	–0.0001 p.u.Hz	14.4	1.6×10^{-5}	2
$\Delta P_{Tie\text{-}21OPID}$	8.3×10^{-3} p.u.	207.06	0.06	–
$\Delta P_{Tie\text{-}21OFOPID}$	-7.8×10^{-5} p.u.	164.9	0.002	–

Table 6. Comparitive table of numerous studies on the LFC.

Ref.	Controller	Saturation	Deadband	Optimization	Settling time improv.	Peak value improv.	Area of load disturbance
This study	OFOPID	Included	Included	Ant-colony	+51.53%	+1.00%	Area1 only
The study	OFOPID	Included	Included	Ant-colony	+52.6%	+50%	Area2 only
This study	OFOPID	Included	Included	Ant-colony	+97.07%	+85.0%	Area1
This study	OFOPID	Included	Included	Ant-colony	+94.96%	+97.44%	Area2
[18]	PID	Not included	Not included	GOA & ANN	+55.4%	+91.9%	Area1 only
[19]	SMC	Not included	Not included	GWO&PSO	+50%	+85%	Area1 only
[19]	SMC	Not included	Not included	GWO&PSO	+50%	+85%	Area2 only
[19]	SMC	Not included	Not included	GWO&PSO	+50%	+75%	Area1
[19]	SMC	Not included	Not included	GWO&PSO	+50%	+75%	Area2
[20]	Fuzzy PID	Not included	Not included	TDE	+52%	+60%	Area1 only
[21]	PID	Not included	Not included	Jaya algorithm	+50%	+64%	Area1 only
[22]	PID	Not included	Included	Fuzzy	+54%	+86%	Area1 only
[23]	AFOFPID	Not included	Not included	CGO	+58.7%	+88.9%	Area1
[23]	AFOFPID	Not included	Not included	CGO	+62.95%	+98%	Area2
[24]	FOPID	Not included	Not included	IGBO&PSO&WOA	+55%	+64%	Area1
[24]	FOPID	Not included	Not included	IGBO&PSO&WOA	+55%	+62%	Area2

Note: All performance values are expressed as percentage improvements in settling time and peak value relative to each study's baseline controller, ensuring consistent comparison across different optimization criteria (e.g., ITAE, ISE, or time-domain indices).

7. Conclusions and future work

This study presented the design of an Optimized Fractional Order Proportional-Integral-Derivative (OFOPID) controller and an Optimized Proportional-Integral-Derivative (OPID) controller for two-areas interconnected Iraqi power system. The optimal parameters for both controllers were determined using the Ant Colony Optimization (ACO) algorithm. The performance of the proposed OFOPID controller was evaluated under three case studies: a load disturbance of (di = 0.1) was applied to area 1 only, the same disturbance was applied to area 2 only, then, applied to both areas simultaneously.

The findings from three case studies clearly indicated that the proposed OFOPID controller consistently surpassesed the conventional OPID controller in terms of settling time, overshoot mitigation, and suppression of frequency drift. In Case Study 1, the OFOPID reduced the settling time in Area 1 from 18.1 seconds using (OPID) to 8.8 seconds, while also decreasing the peak value from 4.495×10^{-4} to 4.45×10^{-4}. In Case Study 2, the OFOPID shortened the settling time in Area 2 from 27.8 seconds to 13.1 seconds and reduced the peak value to -0.0001 p.u. In Case Study 3, the OFOPID achieved the fastest stabilization where the settling was reached in just 14.4 seconds in Area 2 compared to 285.7 seconds for the OPID, while maintaining minimal frequency deviation. The controller's robustness was validated by a nonlinear model incorporating governor dead-band and generation-rate limitations, so ensuring realistic performance. Nonetheless, its scalability to more complex or renewable-integrated systems and the possibility of real-time application remain unresolved difficulties. Future work efforts will focus on these elements via adaptive extensions and hardware-in-the-loop validation to verify the controller's efficacy in practical applications.

Acknowledgment

The authors declare that no external funding was received for this research.

Conflict of interest

The authors declare no conflict of interest.

Data availability

The data that support the findings of this study are available on request from the corresponding author.

References

[1.] S. K. Ojha and C. O. Maddela, "Load frequency control of a two-area power system with renewable energy sources using brown bear optimization technique," *Electrical Engineering,* vol. 106, no. 3, pp. 3589–3613, 2024.
[2.] N. K. Gupta, M. K. Kar, and A. K. Singh, "Load Frequency Control of Two-Area Power System by Using 2 Degree of Freedom PID Controller Designed with the Help of Firefly Algorithm," *Singapore*, pp. 57–64, 2021.
[3.] V. N. Ogar, S. Hussain, and K. A. A. Gamage, "Load Frequency Control Using the Particle Swarm Optimisation Algorithm and PID Controller for Effective Monitoring of Transmission Line," vol. 16, no. 15, p. 5748, 2023.
[4.] V. V. Huynh *et al.*, "Load Frequency Control for Multi-Area Power Plants with Integrated Wind Resources," vol. 11, no. 7, p. 3051, 2021.
[5.] Z. Hamodat and G. Cansever, "Automated Generation Control of Multiple-Area Electrical System with an Availability-Based Tariff Pricing Scheme Regulated by Whale Optimized Fuzzy PID Controller," vol. 2021, no. 1, p. 5596527, 2021.
[6.] D. K. Gupta, A. V. Jha, B. Appasani, A. Srinivasulu, N. Bizon, and P. Thounthong, "Load Frequency Control Using Hybrid Intelligent Optimization Technique for Multi-Source Power Systems," vol. 14, no. 6, p. 1581, 2021.
[7.] D. M. Andrade, S. Gamboa, and J. A. Torres, "Distributed Load-Frequency Control in Power Systems," in *2020 IEEE ANDESCON*, 2020, pp. 1–6.
[8.] R. Asghar, F. Riganti Fulginei, H. Wadood, and S. Saeed, "A Review of Load Frequency Control Schemes Deployed for Wind-Integrated Power Systems," vol. 15, no. 10, p. 8380, 2023.
[9.] O. Can and M. S. Ayas, "Gorilla troops optimization-based load frequency control in PV-thermal power system," *Neural Computing and Applications,* vol. 36, no. 8, pp. 4179–4193, 2024/03/01 2024.
[10.] I. A. Khan, H. Mokhlis, N. N. Mansor, H. A. Illias, L. Jamilatul Awalin, and L. Wang, "New trends and future directions in load frequency control and flexible power system: A comprehensive review," *Alexandria Engineering Journal,* vol. 71, pp. 263–308, 2023/05/15/2023.
[11.] D. Murugesan, P. Shah, K. Jagatheesan, R. Sekhar, and A. J. Kulkarni, "Cohort intelligence optimization based controller design of isolated and interconnected thermal power system for automatic generation control," in *2022 Second International Conference on Computer Science, Engineering and Applications (ICCSEA)*, 2022, pp. 1–6.
[12.] Z. A. Obaid, L. M. Cipcigan, L. Abrahim, and M. T. Muhssin, "Frequency control of future power systems: reviewing and evaluating challenges and new control methods," *Journal of Modern Power Systems and Clean Energy,* vol. 7, no. 1, pp. 9–25, 2019/01/01 2019.
[13.] N. Hakimuddin, I. Nasiruddin, T. S. Bhatti, and Y. Arya, "Optimal Automatic Generation Control with Hydro, Thermal, Gas, and Wind Power Plants in 2-Area Interconnected Power System," *Electric Power Components and Systems,* vol. 48, no. 6–7, pp. 558–571, 2020/08/06 2020.
[14.] D. K. Gupta *et al.*, "Fractional order PID controller for load frequency control in a deregulated hybrid power system using Aquila Optimization," *Results in Engineering,* vol. 23, p. 102442, 2024/09/01/2024.
[15.] A. K. Maurya, D. Singh, H. Khan, and P. Kumar, "Application of PID Controller Tuning Method for Load Frequency Control in Multi Area Power System at Different Load Conditions," in *2024 International Conference on Integrated Circuits, Communication, and Computing Systems (ICIC3S)*, 2024, vol. 1, pp. 1–6.
[16.] R. Pal, M. M. Sati, T. Pal, A. Singh, S. Vijay, and S. Goyal, "Comparative Analysis of Load Frequency Control Strategies: PID, Fuzzy Logic, and Model Predictive Control (MPC)," in *2024 4th International Conference on Advance Computing and Innovative Technologies in Engineering (ICACITE)*, 2024, pp. 1829–1835.

[17.] M. Ayaz, Dur–e–Zehra, S. M. H. Rizvi, and M. Akbar, "Optimal Load Frequency Control Using Particle Swarm Optimization for Power System Stability," in *2024 International Conference on Engineering & Computing Technologies (ICECT)*, 2024, pp. 1–6.
[18.] M. K. Debnath, R. Agrawal, S. R. Tripathy, and S. Choudhury, "Artificial neural network tuned PID controller for LFC investigation including distributed generation," vol. 33, no. 5, p. e2740, 2020.
[19.] A. Kumar, M. N. Anwar, and S. Kumar, "Sliding mode controller design for frequency regulation in an interconnected power system," *Protection and Control of Modern Power Systems,* vol. 6, no. 1, p. 6, 2021/02/26 2021.
[20.] N. Jalali, H. Razmi, and H. Doagou-Mojarrad, "Optimized fuzzy self-tuning PID controller design based on Tribe-DE optimization algorithm and rule weight adjustment method for load frequency control of interconnected multi-area power systems," *Applied Soft Computing,* vol. 93, p. 106424, 2020/08/01/2020.
[21.] S. Pahadasingh, C. Jena, C. K. Panigrahi, and B. P. Ganthia, "JAYA Algorithm-Optimized Load Frequency Control of a Four-Area Interconnected Power System Tuning Using PID Controller," *Engineering, Technology & Applied Science Research,* vol. 12, no. 3, pp. 8646–8651, 06/06 2022.
[22.] B. Dhanasekaran, J. Kaliannan, A. Baskaran, N. Dey, and J. M. R. S. Tavares, "Load Frequency Control Assessment of a PSO-PID Controller for a Standalone Multi-Source Power System," vol. 11, no. 1, p. 22, 2023.
[23.] M. Barakat, "Novel chaos game optimization tuned-fractional-order PID fractional-order PI controller for load–frequency control of interconnected power systems," *Protection and Control of Modern Power Systems,* vol. 7, no. 1, p. 16, 2022/05/01 2022.
[24.] P. Wang, X. Chen, Y. Zhang, L. Zhang, and Y. Huang, "Fractional-Order Load Frequency Control of an Interconnected Power System with a Hydrogen Energy-Storage Unit," vol. 8, no. 3, p. 126, 2024.
[25.] M. o. I. Electricity, "Annual report of Iraqi Electricity," https://moelc.gov.iq/?page=2879, 2019.
[26.] Z. Zhang and H. Zhang, "Fractional-Order Sliding Mode with Active Disturbance Rejection Control for UAVs," vol. 15, no. 2, p. 556, 2025.
[27.] H. I. Abdulameer and M. J. Mohamed, "Fractional Order Fuzzy Like PID Controller Design for Three Links Rigid Robot Manipulator," *Iraqi Journal of Computers, Communications, Control and Systems Engineering*, vol. 22, no. 4, pp. 80–98, 2022.
[28.] S. Y. Yousif and M. J. Mohamed, "Design of Robust FOPI-FOPD Controller for Maglev System Using Particle Swarm Optimization," *Engineering and Technology Journal*, vol. 39, no. 4A, pp. 653–667, 2021.
[29.] L. T. Rasheed and A. S. Al-Araji, "A Cognitive Nonlinear Fractional Order PID Neural Controller Design for Wheeled Mobile Robot based on Bacterial Foraging Optimization Algorithm," *Engineering and Technology Journal*, vol. 35, no. 3A, pp. 289–300, 2017.
[30.] E. K. Ibrahim, S. A. Gitaffa, and A. H. Issa, "Design of FOPID Controller for DC Motor Speed Control Using Intelligent Swarm Techniques," *4th International Conference on Current Research in Engineering and Science Applications (ICCRESA)*, pp. 40–46, 2022.
[31.] E. K. Ibrahim, A.H. Issa, and S.A. Gitaffa, "Optimization and performance analysis of fractional order PID controller for dc motor speed control," *Journal Européen des Systèmes Automatisés,* vol. 55, no. 6, pp. pp. 741–748., 2022.